Water Quality Research Journal

Water Quality Research Journal Vol 58 No 3, 215 doi: 10.2166/wqrj.2023.011

Efficient removal of perfluorinated compounds with the polyamide nanofiltration membrane and membrane fouling resistance analysis

Yuyang Wu

College of Environment, Hohai University, Nanjing 210098, China
E-mail: 2014050121@hhu.edu.cn

ABSTRACT

Perfluorinated compounds (PFCs) are significant pollutants known for their high toxicity and resistance to natural degradation, posing a severe threat to both the global environment and human health. In this study, a polyamide (PA) membrane with an intermediate layer structure of MXene-TiO_2 (referred to as MXT-NFM) was utilized for the removal of PFCs. Experimental results confirm that MXT-NFM exhibited remarkable capacity in intercepting PFCs, accompanied by the high water flux. To gain insights into the mechanisms governing membrane fouling induced by PFCs, inorganic ions, and organics, a series of fouling tests were conducted using MXT-NFM under diverse conditions. Additionally, the XDLVO theory was employed to provide a theoretical perspective on the interactions occurring during the fouling process. The findings suggest that the MXene-TiO_2 intermediate layer contributed to the exceptional hydrophilicity and rough surface properties, enabling multiple functionalities. These include alleviating membrane pore plugging, improving the physical configuration of the PA layer, and effectively mitigating fouling phenomena in coexisting systems during practical applications. Moreover, the particle size of pollutant colloids and the acid–base interaction were identified as decisive factors influencing the development of membrane fouling.

Key words: membrane fouling, MXene-TiO_2 intermediate layer, nanofiltration membrane, perfluorinated compounds, XDLVO theory

HIGHLIGHTS

- Perfluorinated compounds (PFCs) were efficiently removed by MXene-TiO_2 interlayered nanofiltration membrane.
- Influences of various parameters on the PFCs removal were investigated.
- Influences of various conditions on the membrane fouling were studied.
- Mechanism of membrane fouling was analyzed by the XDLVO theory.

GRAPHICAL ABSTRACT

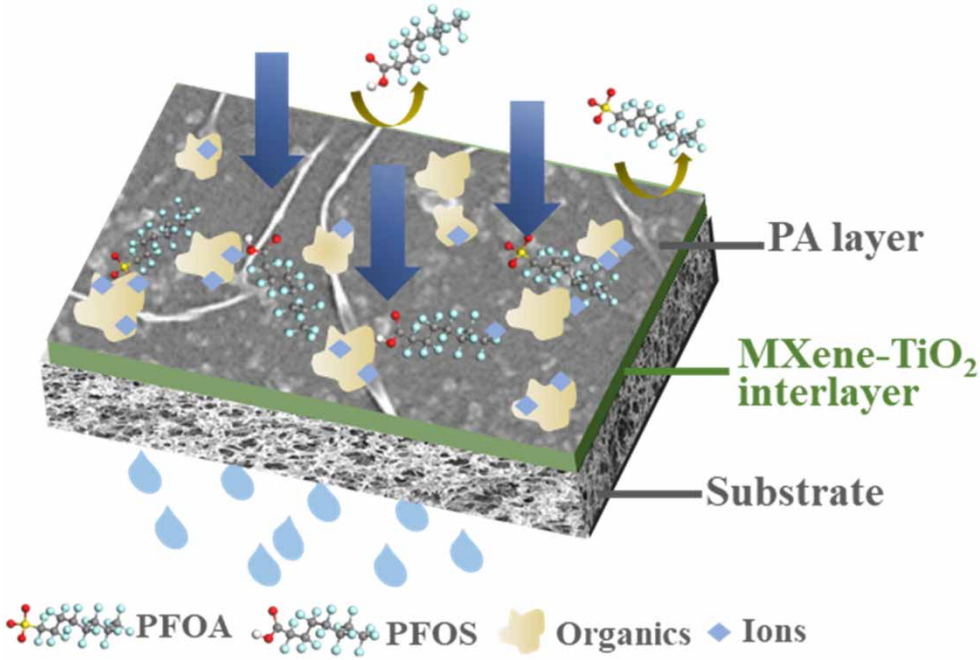

1. INTRODUCTION

Perfluorinated compounds (PFCs), as synthetic substances, have been widely applied in various industries such as chemicals, textiles, leather, and fire extinguishing foams, due to their unique properties of high chemical stability, surface activity, and thermal resistance (Banks *et al.* 2020; Zhang *et al.* 2021; Jl *et al.* 2022). However, in recent years, PFCs have raised increasing concerns regarding their impact on the global environment and human health, primarily ascribed to their toxicity, adverse effects, and resistance to biodegradation in the environment (Pasecnaja *et al.* 2022). As a class of persistent organic pollutants, the presence of aqueous solutions containing hazardous PFCs in our main water sources has become a matter of great concern, as it can potentially lead to significant adverse effects as well as pose risks of diseases and disorders to both abiotic and biotic ecosystems (Zhang *et al.* 2013; Jz *et al.* 2021; Pang *et al.* 2022). Among the various perfluorinated organic pollutants, perfluorooctanoic acid (PFOA) and perfluorooctane sulfonate (PFOS) are two of the most prevalent and representative compounds. Due to their strong polarity and thermal stability, they are highly resistant to degradation by natural factors such as ultraviolet irradiation, chemical reactions, and microbial metabolism (Boo *et al.* 2018; Yang *et al.* 2020; Yuan *et al.* 2020; Tian *et al.* 2021). Consequently, there is an urgent need to develop efficient and reliable techniques for the removal of PFOA and PFOS from aquatic environments.

To date, various technologies have been employed for the removal of PFCs from water, including advanced oxidation, photocatalysis, adsorption, and membrane separation (Tang *et al.* 2007; Meragawi *et al.* 2020; Ding *et al.* 2023). Among these technologies, nanofiltration (NF) membrane technology stands out as a promising option for the efficient removal of PFCs due to its high selectivity and reliability (Steinle-Darling & Reinhard 2008; Park *et al.* 2017). Commercial polymeric NF membranes have shown the ability to remove nearly 90% of PFOA or PFOS. However, the trade-off between permeability and selectivity remains a significant challenge for the widespread application of NF technology (Meng *et al.* 2021; Kwon *et al.* 2022).

Two-dimensional transition metal carbides, nitrides, or carbonitrides (MXene), as a novel type of two-dimensional material, possess abundant surface hydrophilic functional groups, such as hydroxyl and epoxy groups, which bring it excellent hydrophilicity. When used as the interlayer during the preparation of polyamide (PA) NF membranes, these properties contribute to reducing pore blockage in membranes and promoting the uniform distribution of monomers in the aqueous phase during interfacial polymerization, thereby preventing penetration into the membrane pores and resulting in a thinner PA layer (Naguib *et al.* 2011; Jun *et al.* 2019; Peng *et al.* 2019; Wu *et al.* 2020; Xu *et al.* 2020). Considering the rough surface and

hydrophilicity of *in situ* produced MXene-TiO_2 via PMS oxidation, it is desirable to utilize MXene-TiO_2 as an intermediate layer to enhance the performance of the PA layer, achieving a smaller thickness, larger specific surface area, higher flux, and excellent salt cutoff rate. The tunable interlayer channels hold the potential to further improve the trade-off between permeability and selectivity for PFCs removal (Li *et al.* 2017a; Ding *et al.* 2020; Gao *et al.* 2020a, 2020b; Long *et al.* 2021).

Membrane fouling is a process in which pollutants accumulate within the membrane pores or on the membrane surface during the separation process, primarily due to the interaction between the pollutants and the membrane (Liu *et al.* 2023). This phenomenon often leads to pore blockage and the formation of a cake layer, resulting in increased resistance to membrane permeability (Chang *et al.* 2002; Pei *et al.* 2006; Wang *et al.* 2009). In natural water environments, the composition of pollutants is complex, involving the coexistence of organic substances and ions, which poses a significant challenge to the stable purification of NF membranes (Liu *et al.* 2022; Ma *et al.* 2022). During the process of PFCs removal, membrane fouling is also observed (Saravia *et al.* 2006). Therefore, when employing MXT-NFM for PFCs removal, it is crucial to consider the occurrence of membrane fouling in the presence of PFCs and other substances. Humic acid (HA), as one of the natural organic matter (NOM) components in water, is a major contributor to membrane fouling and can affect the removal of PFCs due to enhancement of scaling effect by its hydrophilic functional groups (Guan *et al.* 2018; Li *et al.* 2020). Additionally, cations can also influence membrane fouling. For example, calcium ion (Ca^{2+}), a common cation, can interact with other pollutants, thereby affecting the structure and deposition rate of the filter cake layer and exacerbating membrane fouling (Sutzkover-Gutman *et al.* 2010; Fei & Shih 2011; Miao *et al.* 2017). Therefore, in this study, HA, as a representative of common organic compounds, and Ca^{2+}, as typical ions, will be investigated to explore their role in PFCs removal and to verify whether MXT-NFM exhibits excellent membrane fouling resistance in complex systems (Wang *et al.* 2020). Furthermore, the membrane fouling mechanism of PFCs in coexistence systems has not been clearly defined in current research. Therefore, the extended Derjaguin-Landau-Verwey-Overbeek (XDLVO) theory, a cutting-edge analytical method, will be employed to evaluate the development trend and dominant factors of membrane fouling. The objective is to gain a scientific understanding of the mechanism underlying membrane fouling (Ojaniemi *et al.* 2012; Gao *et al.* 2019).

In this study, we fabricated an NF membrane, MXT-NFM, with MXene-TiO_2 as the intermediate layer structure for the purification of PFCs in aqueous solutions. The presence of the MXene-TiO_2 intermediate layer alleviated membrane pore plugging and resulted in the formation of a thinner and more uniform PA layer. These structural modifications contributed to enhanced water transport and selectivity (Hitsov *et al.* 2015; Gao *et al.* 2020a, 2020b; Wang *et al.* 2023). Experimental results demonstrate that MXT-NFM exhibited high removal efficiency and flux for PFCs. Moreover, the presence of Ca^{2+} and HA enhances the rejection of PFCs, and a higher concentration of Ca^{2+} reduced membrane fouling. The XDLVO theory was employed to evaluate the interaction between pollutants and the membrane, revealing that the particle size of pollutant colloids and the acid–base interaction play crucial roles during the membrane fouling development process. These experimental findings confirmed the excellent performance of MXT-NFM in removing PFCs and mitigating the adverse effects associated with membrane fouling.

2. MATERIALS AND METHODS

2.1. Materials

Ti_3AlC_2 powder, lithium fluoride (LiF, >99.0%), sodium chloride (NaCl, >99.0%), sodium sulfate (Na_2SO_4, >99.0%), hydrochloric acid (HCl, 32%), anhydrous piperazine (PIP, >99.0%), trimesoyl chloride (TMC, >99.0%), perfluorooctanoic acid (PFOA, >99.0%), perfluorooctane sulfonate (PFOS, >99.0%), humic acid (HA, >99.0%), potassium monopersulfate (PMS, >99.0%), and *N*-Hexane (C_6H_{14}, >99.0%) were purchased from Shanghai Aladdin Biochemical Technology Co, Ltd. A polyethersulfone (PES) microfiltration membrane with a nominal pore size of 0.22 μm was used as the substrate. All reagents used in this study are of analytical grade and used without further purification. Milli-Q deionized water with a resistivity of 18.1 MΩ cm at 25 °C was used for the preparation of all solutions.

2.2. Synthesis of $Ti_3C_2T_x$ nanosheets and MXene-TiO_2

$Ti_3C_2T_x$ nanosheets were synthesized *in situ* using a mild HF method. In a typical procedure, 1 g of LiF was added to 15 mL of HCl (6 M), and the mixture was continuously stirred for 5 min. Then, 1 g of Ti_3AlC_2 powder was gradually added to the etchant and the reaction was carried out at 35 °C for 24 h. Subsequently, the resulting mixture was washed by deionized water with centrifugation for 5 cycles to achieve neutral pH. The black $Ti_3C_2T_x$ slurry was collected and redispersed in

100 mL of deionized water. The mixture was then sonicated under flowing nitrogen for 1 h to achieve delamination and followed by centrifugation at 3,500 rpm for 30 min.

For the preparation of MXene-TiO_2, a PMS solution was added to the MXene solution in a mass ratio of 25:1. The mixture was then mixed with a small amount of deionized water and transferred to a centrifuge tube. Ultrasonication was carried out for 5 min until the solution became clear and colorless, resulting in the desired MXene-TiO_2 solution. To prevent any interference from oxidation, the solution should be used immediately after preparation.

2.3. Fabrication of NF membrane

To prepare the PIP-based PA layer, a PIP aqueous solution with a mass fraction of 0.75 wt% was first prepared. Subsequently, a TMC oil phase solution with a mass fraction of 0.038 wt% was prepared by dissolving TMC into *N*-hexane.

The PES substrate, which had been pre-soaked in deionized water, was then naturally dried and placed into a self-made mold. The aqueous solution was poured into the mold and kept for 5 min. Excess solution was then poured out, and any residual solution on the membrane surface was wiped clean.

Next, the oil phase solution was poured onto the membrane and left to react for 2 min. Afterward, the excess solution was removed, and the membrane was taken out and soaked in deionized water for 2 min to remove any residual reagent. The pure PA NF membrane was obtained by placing the cleaned base membrane into an 80 °C vacuum oven for 3 min and denoted as pure membrane. The membrane was then stored in deionized water for further use.

For the preparation of MXT-NFM, 0.5 mL of the MXene-TiO_2 solution was sprayed onto the base membrane before pouring the aqueous phase. The membrane was allowed to stand for 10 min. Subsequently, it was soaked in deionized water for 30 min and followed by drying in air. The obtained membrane was used as the substrate for the preparation of MXT-NFM, and the remaining steps followed the same process as the preparation of the pure membrane.

2.4. Characterizations

X-ray diffraction (XRD) analysis was conducted over the 2θrange of 5-70° with the scanning rate of 0.2 s step^{-1}. Morphologies of MXene nanosheets and MXene-TiO_2 were characterized by high-resolution transmission electron microscopy (HRTEM; FEI Tecnai G2 F20, Japan). The micrographs of membranes were visualized by the field emission scanning electron microscope (FESEM; Hitachi S4800, Japan). Fourier transform infrared spectroscopy (FTIR; TENSOR 27, Bruker, Germany) was applied to investigate the near-surface functional groups of samples within a scanning range of 100–4,000 cm^{-1}. Atomic force microscopy (AFM; NSG10, NT-MDT, ca. 330 kHz) was further employed to assess the membrane surface roughness. Water contact angles were tested on a contact angle measurement system (CAM200) to evaluate the hydrophilcity of membrane surface. The Anton Paar SurPASS electrokinetic analyzer was used to detect the zeta potential of the as-prepared NF membranes by using KCl aqueous solution (1 mM, pH = 3.0–10.0).

2.5. Membrane performance testing

The NF performance tests of the prepared membranes were conducted using a custom-made test unit (Figure 1). A stainless steel membrane module with an effective membrane area of 34.03 cm^2 was used to hold the membrane sample. The feed solution, containing Na_2SO_4 at a concentration of 3.5 wt%, was circulated on the feed side of the membrane module using an experimental pressure pump. The system was allowed to stabilize until the flux at the discharge outlet reached a steady state. The discharged liquid was collected, and the desalination performance of the membrane sample was determined.

The membrane's NF performance was evaluated based on its salt rejection and water flux. The water flux (J) was calculated using the following equation:

$$J = \frac{M}{A \times \Delta t} \tag{1}$$

where M is the permeation mass (kg), A is the effective membrane area (m^2), and t is the collecting time (h).

The rejection (R) for salt or PFCs was determined by comparing the ion concentration in the permeate to that in the feed solution. It was calculated using the following equation:

$$R = \frac{C_f - C_p}{C_f} \tag{2}$$

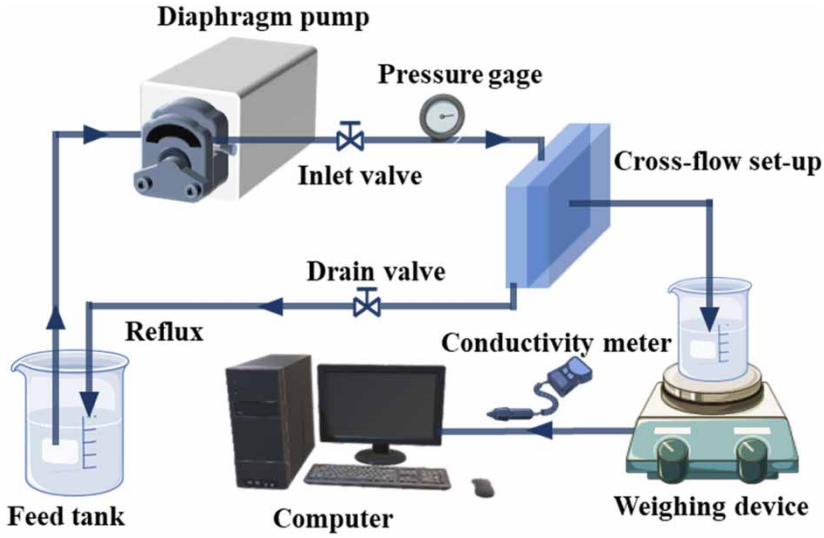

Figure 1 | Homemade test device for nanofiltration.

where C_f and C_p represent the ion conductivity of the permeate and the feed, respectively. The ion concentrations were measured using a portable conductivity meter.

To assess the membrane purification performance toward PFCs, PFOA solution (100 μg/L) and PFOS solution (100 μg/L) were used as the feed solutions. The process described above was repeated, and the purification performance of the membrane was evaluated using Equations (1) and (2). The discharged solutions were collected in injection bottles for precise composition analysis.

3. RESULTS AND DISCUSSION

3.1. Characterizations of nanomaterials and membranes

The XRD patterns in Figure 2(a) confirm the successful formation of the MXene-TiO_2 heterostructure, as indicated by the appearance of a new peak at 25.64 cm^{-1}, corresponding to anatase TiO_2. TEM micrographs in Figure 2(b) and 2(c) reveal the topological structure of MXene nanosheets and MXene-TiO_2. The MXene nanosheets exhibited a nearly transparent and flat surface, while MXene-TiO_2 maintained its laminar structure with abundant small particles decorating the surface.

SEM images of the surface and cross-section of the pure membrane and MXT-NFM in Figure 2(d) and 2(g) demonstrate that the addition of the intermediate layer contributed to the formation of a wrinkled structure in the PA layer, compared to the relatively smooth surface of the pure membrane. The wrinkled structure is primarily attributed to two factors: Firstly, the intermediate layer reduced the pore size of the substrate, hindering water penetration into the pores, and promoting interfacial polymerization on the surface of the PES substrate membrane. Secondly, the hydrophilic functional groups on the intermediate layer reduced the diffusion rate of the PIP monomer in the aqueous phase, resulting in a lower reaction rate with TMC and the formation of the wrinkled structure. Moreover, the addition of the intermediate layer significantly reduced the thickness of the PA layer due to the enhanced interaction between the amine monomers and the hydrophilic MXene-TiO_2, which impeded the diffusion of PIP monomer and its reaction with the organic phase (Figure 2(e) and 2(f)).

AFM images in Figure 2(f) and 2(i) reveal the surface roughness of the NF membranes. The MXT-NFM membrane exhibited a higher surface roughness with an Ra value of 18.31 nm, approximately four times greater than that of the pure membrane. The rougher surface can potentially enhance the permeable area of the PA layer, facilitating more efficient water molecule transport and resulting in water flux improvement.

The chemical structure of MXT-NFM was analyzed using FTIR spectra. As depicted in Figure 3(a), the peak at 1,580 cm^{-1} was attributed to the coupling effect of N–H bond bending vibration and C–N bond elastic vibration in the plane of the –CONH– bond structure, confirming the successful polymerization reaction and the formation of the PA layer on the

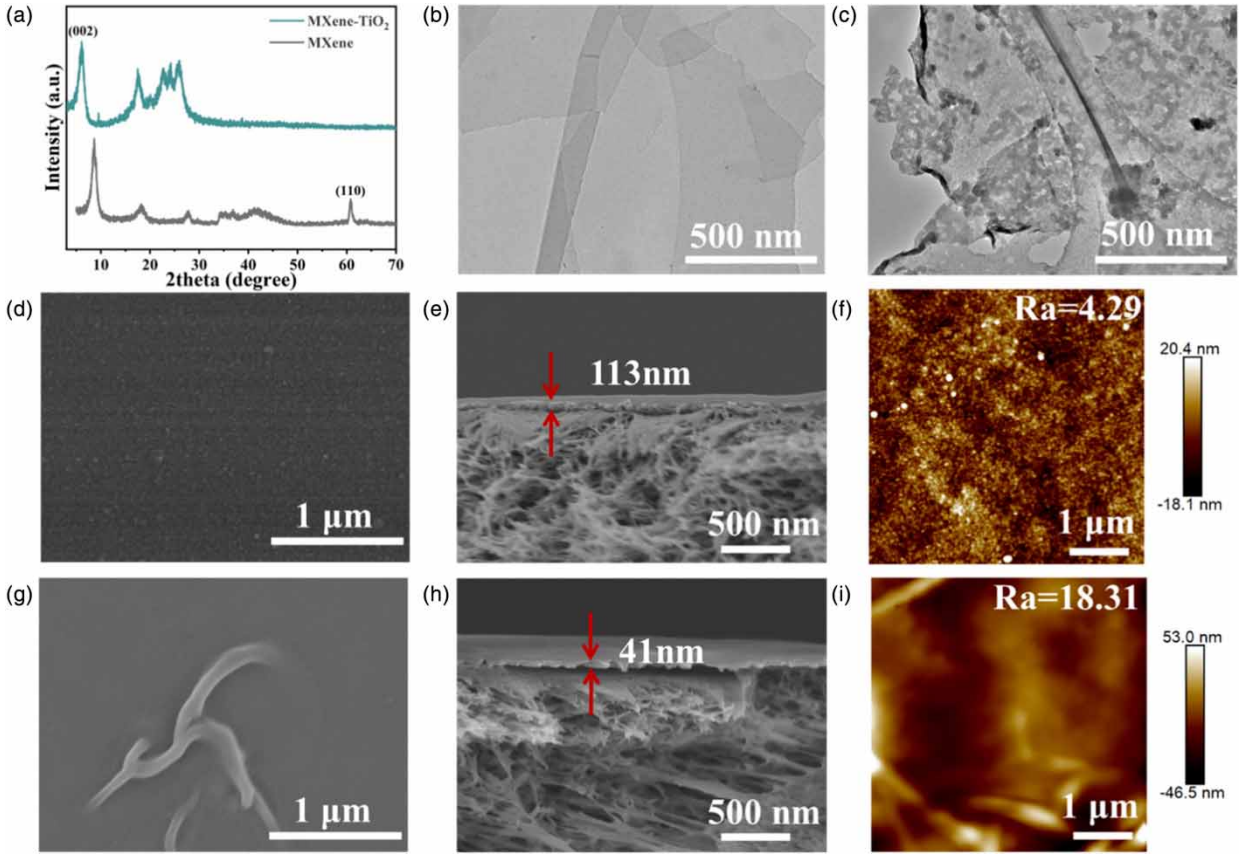

Figure 2 | (a) XRD pattern of nanomaterials. TEM images of (b) MXene nanosheets and (c) MXene-TiO_2. SEM images of the surface and cross-section of (d, e) pure membrane and (g, h) MXT-NFM. AFM images of (f) pure membrane and (i) MXT-NFM.

substrate surface. Additionally, the characteristic peaks of –OH at 3,450 cm^{-1} and –C = O at 1,620 cm^{-1} indicated that the introduced intermediate layer effectively improves the hydrophilicity of the membrane.

Figure 3(b) displays the water contact angles of the pure membrane and MXT-NFM, measuring 44.9°and 22.4°, respectively. Test results indicate that the incorporation of MXene-TiO_2 effectively enhances the hydrophilicity of the NF membrane. This improvement can be attributed to two possible factors: (1) the presence of hydrophilic groups on the surface of MXene-TiO_2 and (2) the intrinsic structure of MXene-TiO_2 provided additional water pathways within the NF membrane, reducing steric hindrance and facilitating water molecule migration and diffusion.

The charged properties of the membrane surface have a significant impact on membrane retention performance. Zeta potential analysis was employed in this study to investigate the difference in surface charge between the pure membrane and MXT-NFM. As illustrated in Figure 3(c), the pure membrane exhibited a negative charge until the pH exceeded 3.2, whereas MXT-NFM displayed a negative charge until the pH exceeded 3.8. The enhanced negative surface charge of MXT-NFM would promote anion repulsion during the process of filtration.

Permeance and rejection toward PFCs of the NF membranes were further investigated. Figure 3(d) demonstrates that the permeance of MXT-NFM was significantly increased, reaching approximately three times that of the pure membrane. This improvement can be attributed to the enhanced hydrophilicity and surface roughness of MXT-NFM. Simultaneously, the rejection of MXT-NFM for PFOA and PFOS was 84.76 and 99.81%, respectively, slightly higher than that of the pure membrane. The higher rejection can be attributed to the more negatively charged surface of MXT-NFM, which strengthened the electrostatic repulsion. Notably, the rejection of PFOS was higher than that of PFOA, primarily due to the larger size of PFOS molecules, which increases steric hindrance while passing through the NF membrane.

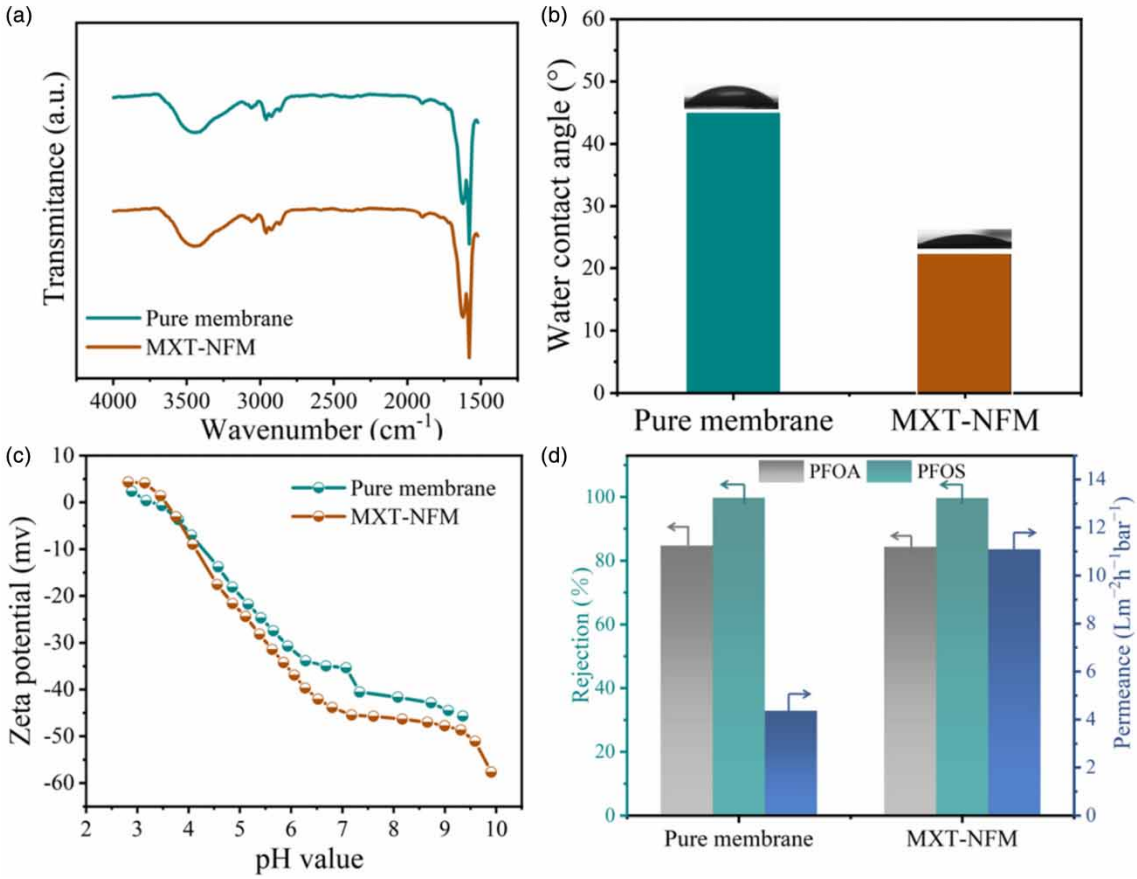

Figure 3 | (a) FTIR spectra, (b) water contact angle, (c) zeta potential, and (d) PFCs rejections as well as permeance of pure membrane and MXT-NFM.

3.2. Influences of the operation parameters on the PFCs removal

3.2.1. Effect of PFCs concentration on PFCs removal

Water samples with various concentrations of PFOS and PFOA (10, 50, 100, and 200 μg/L) were prepared under a constant pressure of 4 bar. As depicted in Figure 4(a), the rejection rates of PFOS and PFOA by the MXT-NFM membrane gradually increased with growing concentration. When the concentration of PFOS increased from 10 to 200 μg/L, the rejections increased from 97.36 to 99.7%. Similarly, when the concentrations of PFOA increased from 10 to 200 μg/L, the rejections of PFOA increased from 85.26 to 94.84%. This phenomenon was probably because the higher initial concentration of PFCs resulted in increased adsorption and deposition of PFOS or PFOA on the membrane surface. Moreover, the increased PFCs concentration facilitated the formation of filter cake layer and improved the screening effect of the NF membrane, thereby enhancing the rejection rates of PFOS and PFOA. Based on these experimental findings, it can be concluded that the growth of PFCs concentration can correspondingly improve the removal efficiency of PFCs by the MXT-NFM membrane.

3.2.2. Effect of initial pH on PFCs removal

The surface charge of the NF membrane plays a crucial role in the removal of charged compounds. It is widely recognized that the membrane charge is closely associated with the pH value of the water sample. Additionally, the pH value of the water sample also affects the chemical forms of organic compounds in water, thereby influencing the interaction between the NF membrane and organic compounds. Accordingly, it is important to investigate the impact of initial pH on the removal of PFCs by the MXT-NFM membrane. As shown in Figure 4(b), the rejections of PFOS and PFOA by the MXT-NFM membrane increased from 94.32 to 99.73% and 82.79 to 95.48%, respectively, as the pH value of the water sample increased from 3 to 10. This indicates that the pH value has a significant influence on the removal efficiency of PFOS and PFOA by the MXT-NFM

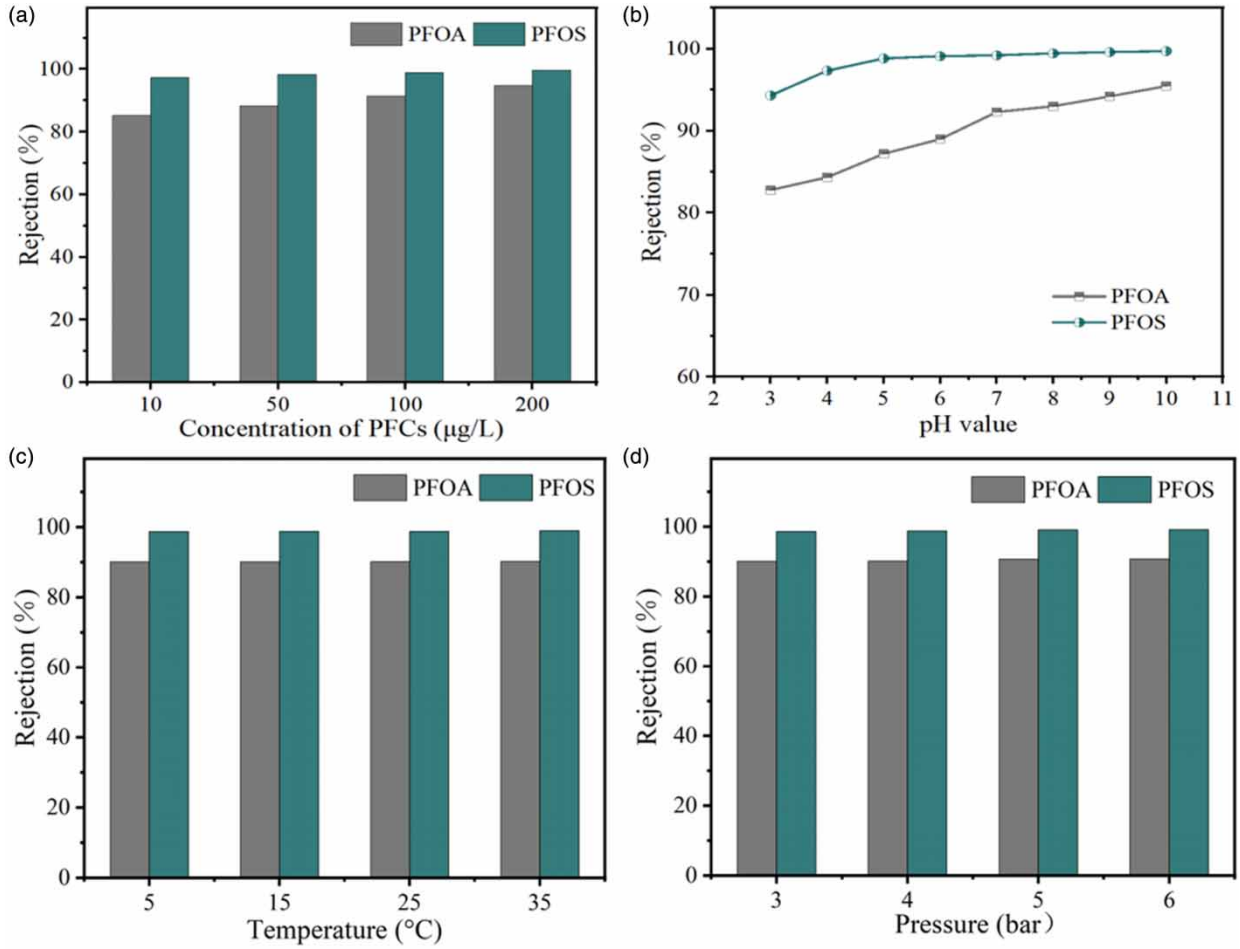

Figure 4 | The influence of (a) PFCs concentrations, (b) pH values, (c) temperature, and (d) operation pressure on the rejection of PFOA and PFOS.

membrane, primarily due to the electrostatic effect. Based on the trend observed in the zeta potential diagram (Figure 3(c)), when the pH value of the MXT-NFM membrane was lower than the isoelectric point, H^+ ions in the water sample neutralized the negative charge on the membrane surface, resulting in a positively charged membrane surface. Conversely, when the pH value was higher than the isoelectric point, the concentration of OH^- ions in the water sample increased, enriching the membrane surface with negative charges. The interaction between the MXT-NFM membrane and PFOS/PFOA is predominantly governed by electrostatic absorption. Under low pH conditions, the enhanced positive charge on the MXT-NFM membrane surface promoted electrostatic absorption, leading to ineffective interception of PFOS and PFOA. Similarly, with the increment of pH value, the charge density of anions increased, contributing to enhanced electrostatic impedance and rejections of these two types of PFCs. In summary, the alkaline environment facilitated the improved removal performance of MXT-NFM for PFOA and PFOS in practical applications.

3.2.3. Effect of temperature on PFCs removal

To evaluate the influence of temperature removal, the initial concentrations of PFOS/PFOA were kept at 100 μg/L, and the water temperature was adjusted within the range of 5–35 °C. Figure 4(c) demonstrates that the change in temperature exhibited relatively negligible effect on the removal of PFCs. Although the diffusion degree of PFCs and water molecules increased with temperature, the impact on the physicochemical properties remained limited.

3.2.4. Effect of operation pressure on PFCs removal

Under the condition of 100 μg/L PFOS/PFOA concentrations, the effect of operation pressure on the removal of PFCs by the MXT-NFM was investigated, as shown in Figure 4(d). The changes in the rejections of both PFOS and PFOA were negligible as the pressure increased from 3 to 6 bar. This result indicates that the intermediate layer could act as a robust membrane skeleton, providing excellent rigid support and effectively preventing excessive deformation to the MXT-NFM structure.

3.3. Evaluation of the membrane fouling

In natural water samples, there is a coexistence of organic compounds and inorganic salt ions. The complexation reactions between those compositions and the occurrence of membrane fouling can impact the removal efficiency of NF membranes for target pollutants. Therefore, it is essential to consider the influence of the coexistence of inorganic salt ions and organic substances when studying the removal efficiency of MXT-NFM for PFCs. In this study, HA and Ca^{2+} were selected as representative substances to investigate the effect of membrane fouling on the removal of PFCs under coexistence conditions.

3.3.1. Effect of the presence of PFCs on membrane fouling

The time-dependent flux behavior of MXT-NFM in the presence of only PFCs (PFOS or PFOA) is presented in Figure 5(a), under a working pressure of 4 bar and a PFOA or PFOS concentration of 100 μg/L. Upon the addition of PFOS or PFOA water samples, a slight decrease in the flux of MXT-NFM was observed. After 60 min of operation, the flux level reached a stable state. Reduction of flux here can be attributed to the adsorption and deposition of PFCs on the MXT-NFM surface, forming a filter cake layer that hindered the diffusion of water molecules and increased permeability resistance. However, the fouling effect observed was minimal due to the low concentration of PFOS and PFOA. Furthermore, it was observed that the flux attenuation for PFOS was slightly higher than that for PFOA. This difference may be attributed to the weaker electrostatic repulsion between the $–SO_3$ group of PFOS and the membrane compared to the –COOH group of PFOA, making it easier for PFOS to be adsorbed on the membrane surface or inside membrane pores. As the adsorption and desorption of PFCs reached equilibrium over a period of operation, the water flux of MXT-NFM began to stabilize. Following hydraulic cleaning, the water flux of MXT-NFM was restored to its initial high level. Moreover, the anti-fouling performance of the MXT-NFM was quantitatively evaluated using four anti-fouling indices: flux recovery ratio (FRR), total fouling rate (R_t), reversible fouling rate (R_r), and irreversible fouling rate (R_{ir}). As shown in Figure 5(b), the values of FRR, R_t, R_r, and R_{ir} for MXT-NFM filtering PFOA solution were 99.64, 2.80, 2.56, and 0.24%, respectively. Similar values were observed for PFOS. These results indicate that PFOS and PFOA primarily underwent reversible adsorption on the surface and inside of MXT-NFM, which can be easily removed through hydraulic cleaning.

3.3.2. Effect of the coexistence of PFCs and HA on membrane fouling

To investigate the impact of organic compound coexistence on membrane fouling, a coexistence condition of 5 mg/L HA and 100 μg/L PFOS/PFOA was employed. The water flux variation is depicted in Figure 5(c). When HA and PFCs coexisted, the flux of MXT-NFM experienced a significant decrease and eventually reached a stable state after a certain period of time. With 2 h filtration process, the flux values for the PFOS/HA and PFOA/HA systems were recorded as 0.928 and 0.945, respectively. In this coexistence scenario, the water flux decay rate of MXT-NFM was consistently higher than that observed for PFCs alone. Several factors might contribute to this phenomenon. Firstly, the central portion of HA molecule consists of hydrophobic aromatic and fatty groups. Driven by hydrophobic interactions and pressure, HA was prone to adsorb onto the membrane surface, forming a dense organic fouling layer. This layer increased the mass transfer resistance and consequently led to a rapid decline in membrane flux. Secondly, the negative charge density of pollutants in the coexistence of HA and PFOS was lower than that in the coexistence of HA and PFOA, resulting in stronger electrostatic repulsion between the latter and MXT-NFM. This stronger repulsion led to a lower membrane flux decay rate in the presence of HA and PFOA. After hydraulic cleaning, the water flux of MXT-NFM was restored to a high level, accompanied by lower irreversible fouling rates (R_{ir}), as shown in Figure 5(d). These test results indicate that the overall anti-fouling performance of MXT-NFM remained at an ideal level, despite the significant initial impact of HA on permeance (Li *et al.* 2017b; Gao *et al.* 2018).

3.3.3. Effect of coexistence of PFCs, Ca^{2+} and HA on membrane fouling

To investigate the impact of coexistence of inorganic salts and organic compounds on water flux attenuation, $CaCl_2$ was selected to simulate the inorganic salt environment in water. The experimental conditions were set as follows: the initial concentrations of PFOS/PFOA, HA, and Ca^{2+} were 100 μg/L, 5 mg/L, and 2 mM. The operation pressure was 4 bar.

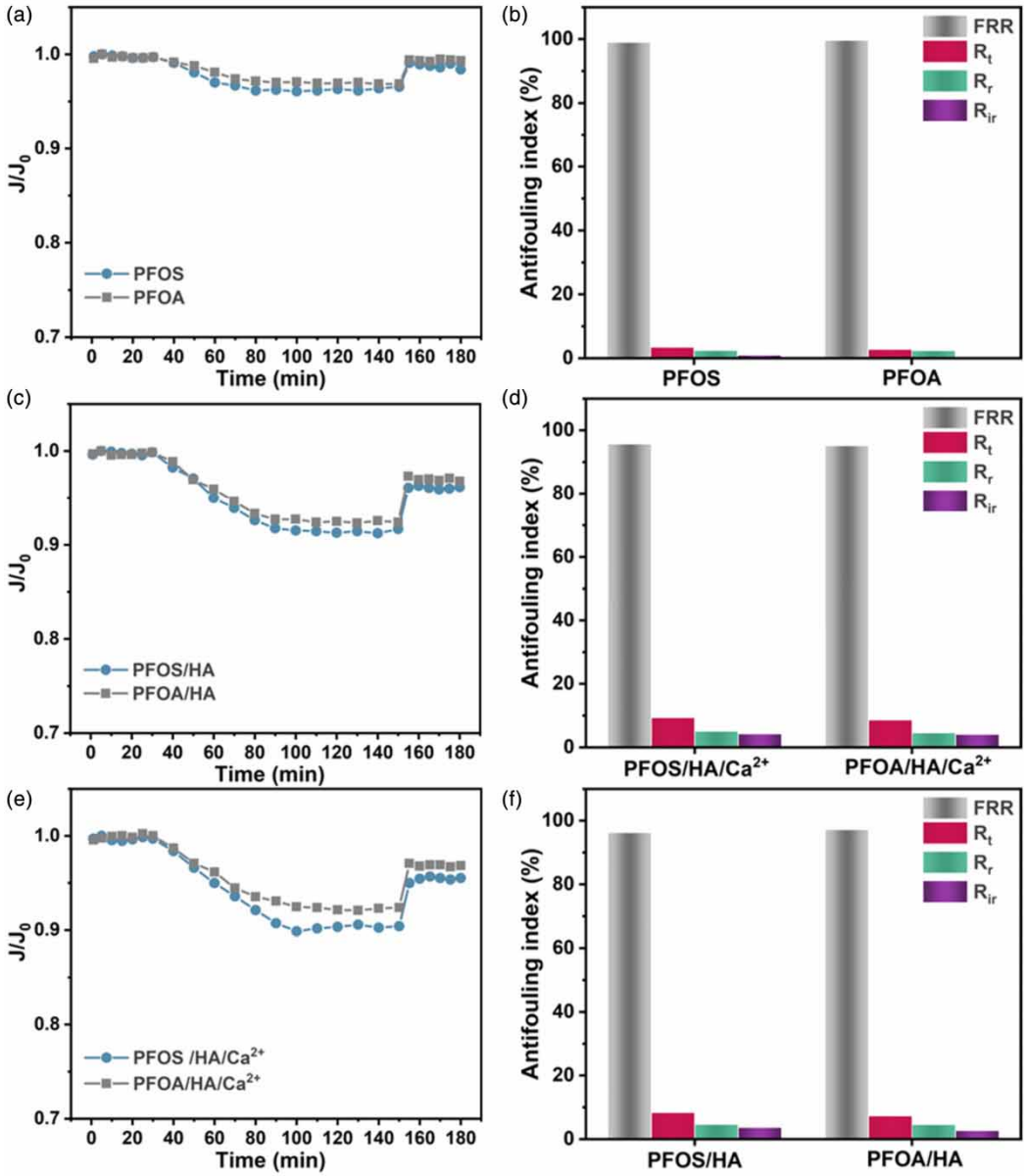

Figure 5 | Time-dependent flux for MXT-NFM and the relative anti-fouling indexes under (a,b) PFCs system, (c,d) PFCs/HA system, and (e,f) PFCs/HA/Ca^{2+} system.

As shown in Figure 5(e), the specific flux of MXT-NFM in the PFCs/HA/Ca^{2+} system exhibited a significant decrease compared with that of the HA/PFCs coexistence system. After 2 h of filtration, the specific flux values were measured as 0.906 for the PFOS/HA/Ca^{2+} coexistence system and 0.917 for the PFOA/HA/Ca^{2+} coexistence system. The reduction was because the addition of Ca^{2+} weakened the negatively charged properties of HA, PFCs, and membrane surface. Consequently, the electrostatic repulsion between MXT-NFM and HA/PFCs decreased, leading to greater aggregation of the two pollutants on the membrane surface. Additionally, the electrostatic repulsive force between the pollutants decreased, resulting in a denser fouling layer on the MXT-NFM surface and a drastic decrease in membrane flux.

As the deposition continued to increase, the adsorption and desorption of pollutants reached an equilibrium state, while the water flux of MXT-NFM approached a stable level. After hydraulic cleaning, the flux recovery remained satisfactory, demonstrating the high anti-fouling performance of MXT-NFM under the coexistence of HA, Ca^{2+}, and PFCs. This can be attributed to the excellent hydrophilicity of MXT-NFM, which facilitated a tight combination between the membrane surface and water

molecules, forming a compact hydration layer and reducing the interaction between pollutants and membrane surface (Shao *et al.* 2011; Chang *et al.* 2012).

3.4. Mechanism analysis of membrane fouling by the XDLVO theory

In general, the membrane fouling process can be divided into two stages: the early stage which is primarily controlled by the interaction between free pollutants and the clean membrane surface, and the later stage which is mainly controlled by the interaction between free pollutants and the pollutants deposited on the membrane surface. To understand more details about the fouling mechanism, the XDLVO theory was applied to evaluate three energy components governing the interaction: van der Waals interaction energy (LW), electrostatic double-layer interaction energy (EL), and acid–base interaction energy (AB). By analyzing these interaction relationships between contaminants and membrane, as well as between contaminants themselves, we can gain insights into the fouling mechanism.

3.4.1. Determination of the surface parameters of membrane and pollutants

Supplementary Table S1 presents the zeta potential, colloid particle size, and contact angles of MXT-NFM and six different pollutant colloids, along with three probe liquids. When PFOS or PFOA coexisted with HA, the contact angle of the colloid decreased, indicating increased hydrophilicity. At the same time, the increased negative zeta potential can be attributed to the presence of carboxyl and hydroxyl groups in HA molecules, which enhanced the hydrophilicity and negative zeta potential of PFOS and PFOA. On the other hand, when Ca^{2+} was added, the contact angle of the colloid and its hydrophobicity increased, while the negative zeta potential decreased. This can be explained by the reaction of Ca^{2+} with PFCs and HA, weakening the negative charge on the carboxyl and hydroxyl groups in HA which resulted in a reduction in the overall hydrophilicity and negative zeta potential of the mixed pollutants. Furthermore, the coexistence of these components resulted in the formation of complex organic compounds with larger particle sizes.

3.4.2. Analysis of condensation free energy

Supplementary Table S2 presents the surface tension parameter and condensation free energy of MXT-NFM under different colloid environments. The surface tension data indicates that both the membrane and contaminants exhibited high electron donor composition (γ^-) and relatively low electron receptor components (γ^+). This implies that both the membrane and colloid possessed a strong electron-donating capacity and negative charged surface. The condensation free energy (ΔG_{sws}) refers to the free energy per unit area when two surfaces of the same material are immersed in a solvent (water) and come into contact with each other. ΔG_{sws} serves as a quantitative index for evaluating the hydrophilicity of membrane and pollutant. The positive value of ΔG_{sws} indicates a hydrophilic surface, while the negative value indicates a hydrophobic surface. Furthermore, a higher absolute value signifies a stronger hydrophilicity or hydrophobicity (Li *et al.* 2019).

Based on the data in Supplementary Table S2, the PFOS/HA and PFOA/HA systems exhibited greater hydrophilicity compared to the single PFOS and PFOA systems. However, the hydrophilicity of PFOS/HA/Ca^{2+} and PFOA/HA/Ca^{2+} systems were lower than that of PFOS/HA and PFOA/HA systems. It is important to note that the condensation free energy alone may not be suitable for quantitatively evaluating the interaction energy between the membrane and the pollutant colloids. Therefore, the interaction energy should be further evaluated to understand the actual relationship between the membrane and the pollutant colloids.

3.4.3. Analysis of interaction energy

According to the XDLVO theory, interaction between the membrane and the pollutant is repulsive if the interaction energy between them is positive, indicating that the membrane repels the colloidal pollutants. Conversely, if the interaction energy is negative, it signifies that the membrane is attractive to the colloidal pollutants. Additionally, a higher positive (or negative) value indicates a smaller (or larger) degree of membrane fouling (Lin *et al.* 2014; Gao 2019).

Supplementary Table S3 presents the interaction energy between MXT-NFM and six types of pollutant colloids. When the interaction distance between the pollutant and the membrane surface was 0.158 nm, the acid–base interaction energy dominated the total interaction energy, which determined the development trend of membrane fouling. Notably, in the presence of PFOA, the electrostatic double-layer interaction energy between membrane and colloid (U_{mlc}^{EL}) value between MXT-NFM and the pollutant was positive, indicating a repulsive electrostatic interaction, which suggests that membrane fouling would be relatively slower. Conversely, when the contaminant contained PFOS, the U_{mlc}^{EL} value between MXT-NFM and the pollutant was negative, possibly due to significant differences in surface charge density. This negative value indicated a certain

attraction between MXT-NFM and the colloids, which was consistent with the trend of membrane flux decay. The particle size of mixed pollutants was significantly larger than that of the single PFOS and PFOA systems, and particle size greatly influenced the magnitude of interface free energy between membrane and colloid ($U_{\mathrm{mlc}}^{\mathrm{XDLVO}}$). A larger particle size

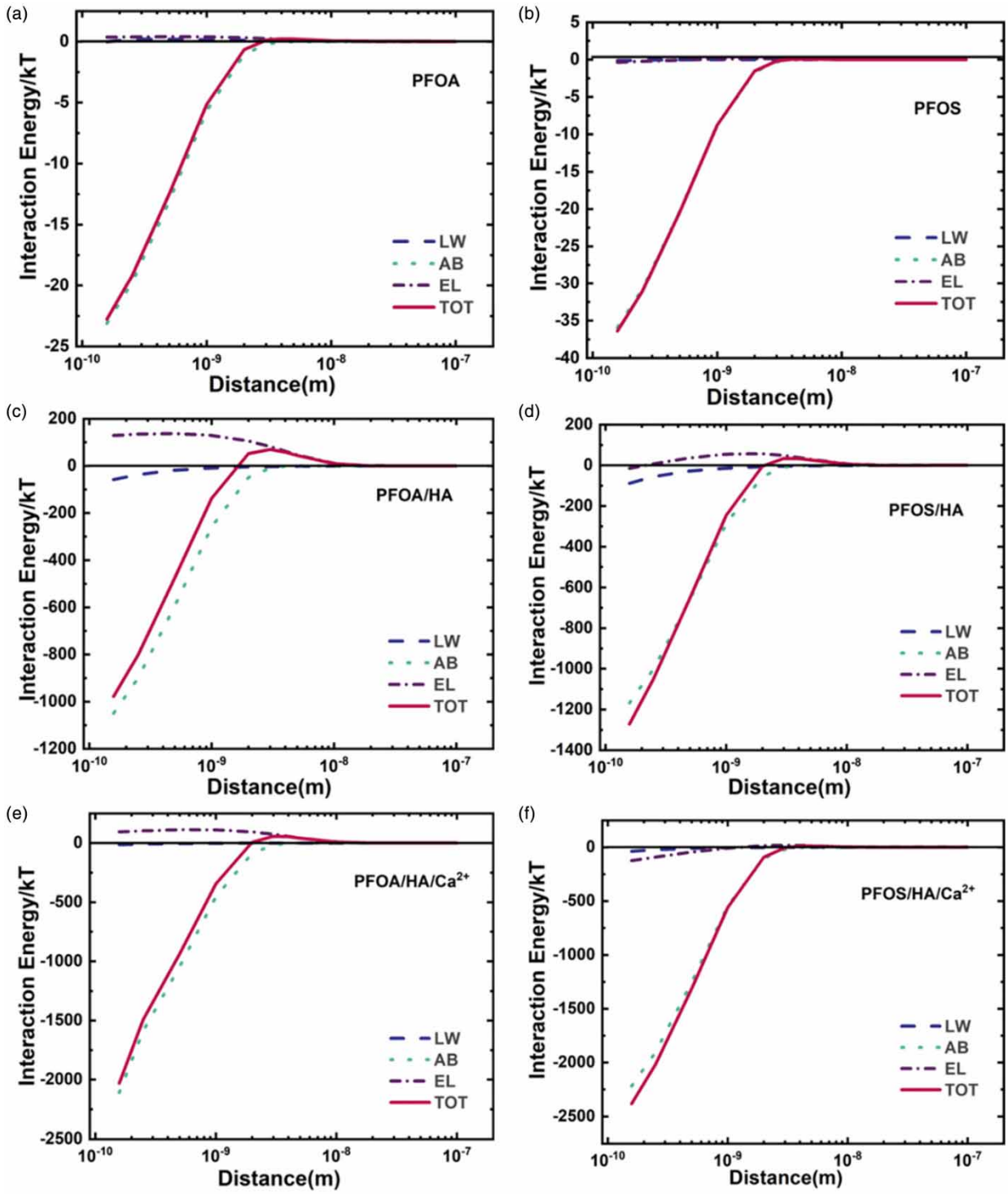

Figure 6 | XDLVO interaction energy profiles for MXT-NFM and colloids under (a) PFOA system, (b) PFOS system, (c) PFOA/HA system, (d) PFOS/HA system, (e) PFOA/HA/Ca^{2+} system and (f) PFOS/HA/Ca^{2+} system.

corresponded to a more negative U_{mlc}^{XDLVO} value and a stronger attractive force between the membrane and the colloid, facilitating colloid particle adsorption on the membrane surface and resulting in more severe membrane fouling.

In the later stage of membrane fouling, the MXT-NFM surface is gradually covered by a fouling layer, wherein the interaction between the pollutants near the membrane surface and the deposited pollutants becomes crucial for membrane fouling. Supplementary Table S3 shows that the U_{mlc}^{XDLVO} between pollutants was negative in the case of single PFCs systems, primarily due to the strong hydrophobicity of PFOA or PFOS, which contributed to the mutual attraction between the pollutants. However, upon adding HA, the U_{mlc}^{XDLVO} of PFOA/HA and PFOS/HA pollutants became positive due to the strong hydrophilicity of HA, leading to mutual exclusion between the pollutants. With the further addition of Ca^{2+}, the U_{mlc}^{XDLVO} maintained a positive value, albeit slightly lower than that of the PFOA/HA and PFOS/HA systems. This decrease was mainly attributed to the reduced hydrophilicity of the pollutants caused by the addition of Ca^{2+}, thereby decreasing the mutual exclusion between the pollutants. Similar to the early stage of membrane fouling, the absolute value of U_{mlc}^{XDLVO} in the coexisting system was significantly higher than that in the single PFCs system, which was mainly attributed to the larger particle size of pollutants in the coexisting system, emphasizing the significant influence of colloid particle size on the interaction energy. Furthermore, as shown in Supplementary Table S4, the acid–base interaction energy still dominated the total interaction energy in the later stage when the interaction distance was 0.158 nm, indicating that the hydrophobic interaction between pollutant colloids determined the development trend of membrane fouling.

3.4.4. Relationship between interaction energy and operating distance

To investigate the impact of interaction energy on membrane fouling, the interaction energy between the membrane surface and pollutants at different interaction distances was calculated. In Figure 6, the XDLVO interaction energy spectrum of MXT-NFM and pollutant colloids was plotted as a function of the interaction distance. At large interaction distances (>5 nm), the interaction energy and its components approached zero. When the interaction distance was smaller than the critical value of the large interaction distance, the proportion of electrostatic interaction energy (EL) and van der Waals interaction energy (LW) was relatively low, exerting minimal influence on the overall interaction energy. However, as the interaction distance decreased from 5 nm to the minimum operating distance of 0.158 nm, the acid–base interaction energy (AB) increased at a faster rate than the electrostatic and van der Waals interaction energies. Consequently, the acid–base interaction energy became the dominant factor and determined the development trend of membrane fouling.

In summary, during the entire process of membrane fouling, the particle size of the pollutant colloids and the acid–base interaction play crucial roles in the development of membrane fouling.

4. CONCLUSIONS

In this study, MXene-TiO_2 was chosen as the intermediate layer of a PA membrane to investigate the practical performance of MXT-NFM in the treatment of PFCs. Experimental findings demonstrate that MXene-TiO_2 interlayer endowed the MXT-NFM with excellent hydrophilicity reduced thickness of the PA layer, thereby overcoming the trade-off effect for PFCs removal. During membrane fouling tests, MXT-NFM demonstrated significant resistance to membrane fouling with high removal efficiency of PFCs in the complex pollutant. The application of the XDLVO theory reveals that colloidal particle size and acid–base interactions were critical factors influencing the development of membrane fouling.

ACKNOWLEDGEMENTS

This work was supported by the Key-Area Research and Development Program of Guangdong Province (2020B0101130001) and the National Natural Science Foundation of China (No. 51978239).

DATA AVAILABILITY STATEMENT

All relevant data are included in the paper or its Supplementary Information.

CONFLICT OF INTEREST

The authors declare there is no conflict.

REFERENCES

Banks, D., Jun, B. M., Heo, J., Her, N., Park, C. M. & Yoon, Y. 2020 Selected advanced water treatment technologies for perfluoroalkyl and polyfluoroalkyl substances: a review. *Sep. Purif. Technol.* **231**, 115925.

Boo, C., Wang, Y., Zucker, I., Choo, Y., Osuji, C. O. & Elimelech, M. 2018 High performance nanofiltration membrane for effective removal of perfluoroalkyl substances at high water recovery. *Environ. Sci. Technol.* **52**, 7279–7288.

Chang, I. S., Clech, P. L., Jefferson, B. & Judd, S. 2002 Membrane fouling in membrane bioreactors for wastewater treatment. *J. Environ. Eng.* **128**, 11.

Chang, E. E., Chang, Y. C., Liang, C. H., Huang, C. P. & Chiang, P. C. 2012 Identifying the rejection mechanism for nanofiltration membranes fouled by humic acid and calcium ions exemplified by acetaminophen, sulfamethoxazole, and triclosan. *J. Hazard. Mater.* **221–222**, 19–27.

Ding, L., Li, L., Liu, Y., Wu, Y., Lu, Z., Deng, J. J., Wei, Y. Y., Caro, J. & Wang, H. H. 2020 Effective ion sieving with $Ti_3C_2T_x$ MXene membranes for production of drinking water from seawater. *Nat. Sustain.* **3**, 296–302.

Ding, M. M., Xu, H., Yao, C., Chen, W., Song, N., Zhang, Q., Lin, T. & Xie, Z. L. 2023 Understanding the membrane fouling control process at molecular level in the heated persulfate activation-membrane distillation hybrid system. *Water Res.* **229**, 119465.

Fei, W. & Shih, K. 2011 Adsorption of perfluorooctane sulfonate (PFOS) and perfluorooctanoate (PFOA) on alumina: influence of solution pH and cations. *Water Res.* **45**, 2925–2930.

Gao, J. D. 2019 Modelling mass and heat transfers of permeate gap membrane distillation using hollow fibre membrane. *Desalination* **467**, 196–209.

Gao, L., Zhang, J., Gray, S. & Li, J. D. 2018 Influence of PGMD module design on the water productivity and energy efficiency in desalination. *Desalination* **452**, 29–39.

Gao, K., Li, T., Liu, J., Dong, B. & Chu, H. 2019 Ultrafiltration membrane fouling performance by mixtures with micromolecular and macromolecular organics. *Environ. Sci.: Water Res. Technol.* **5**, 277–286.

Gao, W., Li, X., Luo, S., Luo, Z. & Luo, M. 2020a In situ modification of cobalt on MXene/TiO_2 as composite photocatalyst for efficient nitrogen fixation. *J. Colloid Interface Sci.* **585**, 20–29.

Gao, L., Li, J., Yang, G., Zhang, J. & Xie, Z. 2020b De-ammonification using direct contact membrane distillation – an experimental and simulation study. *Sep. Purif. Technol.* **250**, 117158.

Guan, Y. F., Qian, C., Chen, W., Huang, B. C., Wang, Y. J. & Yu, H. Q. 2018 Interaction between humic acid and protein in membrane fouling process: a spectroscopic insight. *Water Res.* **145**, 146–152.

Hitsov, I., Maere, T., De Sitter, K., Dotremont, C. & Nopens, I. 2015 Modelling approaches in membrane distillation: a critical review. *Sep. Purif. Technol.* **142**, 48–64.

Jl, A., Jing, S. A. & Pla, B. 2022 Exposure routes, bioaccumulation and toxic effects of per- and polyfluoroalkyl substances (PFASs) on plants: a critical review. *Environ. Int.* **158**, 106891.

Jun, B. M., Kim, S., Heo, J., Chang, M. P., Her, N., Min, J., Huang, Y., Han, J. H. & Yoon, Y. M. 2019 Review of MXenes as new nanomaterials for energy storage/delivery and selected environmental applications. *Nano Res.* **12**, 17.

Jz, A., Zhen, H. B., Li, G. C., Sg, A. & Zx, B. 2021 Study of MOF incorporated dual layer membrane with enhanced removal of ammonia and per-/poly-fluoroalkyl substances (PFAS) in landfill leachate treatment. *Sci. Total Environ.* **806**, 151207.

Kwon, O., Choi, Y., Kang, J., Ji, H. K., Choi, E., Yun, C. W. & Kim, D. W. 2022 A comprehensive review of MXene-based water-treatment membranes and technologies: recent progress and perspectives. *Desalination* **522**, 115448.

Li, D., Wei, Y., Wang, Y., Chen, H. & Wang, H. 2017a A two-dimensional lamellar membrane: MXene nanosheet stacks. *Angew. Chem., Int. Ed.* **56**, 1825–1829.

Li, G., Zhang, J., Gray, S. & Li, J. D. 2017b Experimental study of hollow fiber permeate gap membrane distillation and its performance comparison with DCMD and SGMD. *Sep. Purif. Technol.* **188**, 11–23.

Li, R., Lou, Y., Xu, Y., Ma, G., Liao, B. Q., Shen, L. & Lin, H. J. 2019 Effects of surface morphology on alginate adhesion: molecular insights into membrane fouling based on XDLVO and DFT analysis. *Chemosphere* **233**, 373–380.

Li, B., He, X., Wang, P., Liu, Q. & Ma, J. 2020 Opposite impacts of K^+ and Ca^{2+} on membrane fouling by humic acid and cleaning process: evaluation and mechanism investigation. *Water Res.* **183**, 116006.

Lin, T., Shen, B., Chen, W. & Zhang, X. B. 2014 Interaction mechanisms associated with organic colloid fouling of ultrafiltration membrane in a drinking water treatment system. *Desalination* **332**, 100–108.

Liu, M., Chen, W., Fu, J., Wang, A., Ding, M., Zhang, L., Han, L. & Gao, L. 2022 Hyaluronic acid-modified nanofiltration membrane for ultrahigh water permeance and efficient rejection of PFASs. *Process Saf. Environ. Prot.* **166**, 214–221.

Liu, C., Zhang, G., Zhang, W., Gu, Z. & Zhu, G. 2023 Specifically adsorbed ferrous ions modulate interfacial affinity for high-rate ammonia electrosynthesis from nitrate in neutral media. *Proc. Natl. Acad. Sci. USA* **120**, 2209979120.

Long, Q., Zhao, S., Chen, J., Zhang, Z., Qi, G. & Liu, Z. Q. 2021 Self-assembly enabled nano-intercalation for stable high-performance MXene membranes. *J. Membr. Sci.* **635**, 119464.

Ma, J., Wang, Y., Xu, H., Ding, M. & Gao, L. 2022 MXene ($Ti_3T_2C_x$)-reinforced thin-film polyamide nanofiltration membrane for short-chain perfluorinated compounds removal. *Process Saf. Environ. Prot.* **168**, 275–284.

Meng, B., Liu, G., Mao, Y., Liang, F., Liu, G. & Jin, W. 2021 Fabrication of surface-charged MXene membrane and its application for water desalination. *J. Membr. Sci.* **623**, 119076.

Meragawi, S. E., Akbari, A., Hernandez, S., Mirshekarloo, M. S., Bhattacharyya, D., Tanksale, A. & Majumder, M. 2020 Enhanced permselective separation of per-fluorooctanoic acid in graphene oxide membranes by a simple PEI modification. *J. Mater. Chem. A* **8**, 24800–24811.

Miao, R., Li, X., Wu, Y., Wang, P., Wang, L., Wu, G., Wang, J. & Lv, Y. L. 2017 A comparison of the roles of Ca^{2+} and Mg^{2+} on membrane fouling with humic acid: are there any differences or similarities? *J. Membr. Sci.* **545**, 81–87.

Naguib, M., Kurtoglu, M., Presser, V., Lu, J., Niu, J., Min, H., Hultman, L., Gogotsi, Y. & Barsoum, M. W. 2011 Two-dimensional nanocrystals produced by exfoliation of Ti_3 AlC_2. *Adv. Mater.* **23**, 4248–4253.

Ojaniemi, U., Riihimäki, M., Manninen, M. & Pättikangas, T. 2012 Wall function model for particulate fouling applying XDLVO theory. *Chem. Eng. Sci.* **84**, 57–69.

Pang, H., Dorian, B., Gao, L., Xie, Z., Cran, M., Muthukumaran, S., Sidiroglou, F., Gray, S. & Zhang, J. 2022 Remediation of poly- and perfluoroalkyl substances (PFAS) contaminated soil using gas fractionation enhanced technology. *Sci. Total Environ.* **827**, 154310.

Park, H. B., Kamcev, J., Robeson, L. M., Elimelech, M. & Freeman, B. D. 2017 Maximizing the right stuff: the trade-off between membrane permeability and selectivity. *Science* **356**, 1138–1148.

Pasecnaja, E., Bartkevics, V. & Zacs, D. 2022 Occurrence of selected per- and polyfluorinated alkyl substances (PFASs) in food available on the European market – a review on levels and human exposure assessment. *Chemosphere* **287**, 132378.

Pei, X., Drewes, J. E., Kim, T. U., Bellona, C. & Amy, G. 2006 Effect of membrane fouling on transport of organic contaminants in NF/RO membrane applications. *J. Membr. Sci.* **279**, 165–175.

Peng, J., Chen, X., Ong, W. J., Zhao, X. & Li, N. 2019 Surface and heterointerface engineering of 2D MXenes and their nanocomposites: insights into electro- and photocatalysis. *Chem-US* **5**, 18–50.

Saravia, F., Zwiener, C. & Frimmel, F. H. 2006 Interactions between membrane surface, dissolved organic substances and ions in submerged membrane filtration. *Desalination* **192**, 280–287.

Shao, J., Hou, J. & Song, H. 2011 Comparison of humic acid rejection and flux decline during filtration with negatively charged and uncharged ultrafiltration membranes. *Water Res.* **45**, 473–482.

Steinle-Darling, E. & Reinhard, M. 2008 Nanofiltration for trace organic contaminant removal: structure, solution, and membrane fouling effects on the rejection of perfluorochemicals. *Environ. Sci. Technol.* **42**, 5292–5297.

Sutzkover-Gutman, I., Hasson, D. & Semiat, R. 2010 Humic substances fouling in ultrafiltration processes. *Desalination* **261**, 218–231.

Tang, C. Y., Fu, Q. S., Criddle, C. S. & Leckie, J. O. 2007 Effect of flux (transmembrane pressure) and membrane properties on fouling and rejection of reverse osmosis and nanofiltration membranes treating perfluorooctane sulfonate containing wastewater. *Environ. Sci. Technol.* **41**, 2008–2014.

Tian, D., Geng, D., Mehler, W. T., Goss, G., Wang, T., Yang, S., Niu, Y. S., Zheng, Y. & Zhang, Y. F. 2021 Removal of perfluorooctanoic acid (PFOA) from aqueous solution by amino-functionalized graphene oxide (AGO) aerogels: influencing factors, kinetics, isotherms, and thermodynamic studies. *Sci. Total Environ.* **783**, 147041.

Wang, Z., Wu, Z. & Tang, S. 2009 Extracellular polymeric substances (EPS) properties and their effects on membrane fouling in a submerged membrane bioreactor. *Water Res.* **43**, 2504–2512.

Wang, S., Li, L., Yu, S., Dong, B. & Wang, X. 2020 A review of advances in EDCs and PhACs removal by nanofiltration: mechanisms, impact factors and the influence of organic matter. *Chem. Eng. J.* **406**, 126722.

Wang, A., Xu, H., Fu, J., Lin, T., Ma, J., Ding, M. & Gao, L. 2023 Enhanced high-salinity brines treatment using polyamide nanofiltration membrane with tunable interlayered MXene channel. *Sci. Total Environ.* **856**, 158434.

Wu, X., Ding, M. M., Xu, H., Yang, W., Zhang, K., Tian, H., Wang, H. & Xie, Z. L. 2020 Scalable $Ti_3C_2T_x$ MXene interlayered forward osmosis membranes for enhanced water purification and organic solvent recovery. *ACS Nano.* **14**, 9125–9135.

Xu, D., Zhu, X., Luo, X., Guo, Y. & Liang, H. 2020 MXene nanosheet templated nanofiltration membranes toward ultrahigh water transport. *Environ. Sci. Technol.* **55**, 1270–1278.

Yang, L., He, L., Xue, J., Ma, Y. & Zhang, Z. 2020 Persulfate-based degradation of perfluorooctanoic acid (PFOA) and perfluorooctane sulfonate (PFOS) in aqueous solution: review on influences, mechanisms and prospective. *J. Hazard. Mater.* **393**, 122405.

Yuan, Y., Feng, L., He, X., Liu, X., Xie, N., Ai, Z., Zhang, L. Z. & Gong, J. M. 2020 Efficient removal of PFOA with an In_2O_3/persulfate system under solar light via the combined process of surface radicals and photogenerated holes. *J. Hazard. Mater.* **423**, 127176.

Zhang, C., Hong, Y., Fei, L., Xiang, H. & Qi, Z. 2013 Sorption of short- and long-chain perfluoroalkyl surfactants on sewage sludges. *J. Hazard. Mater.* **260**, 689–699.

Zhang, J., Pang, H., Gray, S., Ma, S. & Gao, L. 2021 PFAS removal from wastewater by in-situ formed ferric nanoparticles: solid phase loading and removal efficiency. *J. Environ. Chem. Eng.* **9**, 105452.

First received 26 May 2023; accepted in revised form 13 July 2023. Available online 27 July 2023